ACS APPLIED MATERIALS & INTERFACES

Research Article

Cite This: ACS Appl. Mater. Interfaces 2018, 10, 27771−27779

www.acsami.org

CVD-Grown $MoSe_2$ Nanoflowers with Dual Active Sites for Efficient Electrochemical Hydrogen Evolution Reaction

Nirul Masurkar, Naresh Kumar Thangavel, and Leela Mohana Reddy Arava*

Department of Mechanical Engineering, Wayne State University, Detroit, Michigan 48202, United States

Supporting Information

ABSTRACT: Due to its unique electronic band characteristics (presence of d-orbital in both Mo and Se atoms), $MoSe_2$ has potential to exhibit high electrical conductivity and superior hydrogen evolution reaction (HER) kinetics when compared to other transition-metal dichalcogenides. Though various strategies were employed earlier to obtain $MoSe_2$ structure with different shapes and morphologies, precise control on achieving both Mo- and Se-edge sites and understanding their interaction with reactants in HER remains to be challenging. Here, we successfully demonstrate the vapor diffusion method to grow highly crystalline $MoSe_2$ nanoflowers on carbon cloth in a vertical orientation. Uniformly dispersed nanoflowers with Mo- and Se-edge sites exhibited remarkable electrocatalytic activity on hydrogen reduction in terms of low Tafel slope and high exchange current density. The existence of a strong interaction between $MoSe_2$ and carbon cloth assists in long-term hydrogen production and confirms the exceptional durability of the catalyst. A comprehensive evidence for hydrogen adsorption on dual active sites, viz., Mo- and Se-edges of $MoSe_2$, is provided using X-ray photoelectron spectroscopy and in situ Raman spectroscopy containing a specially designed liquid immersion objective lens.

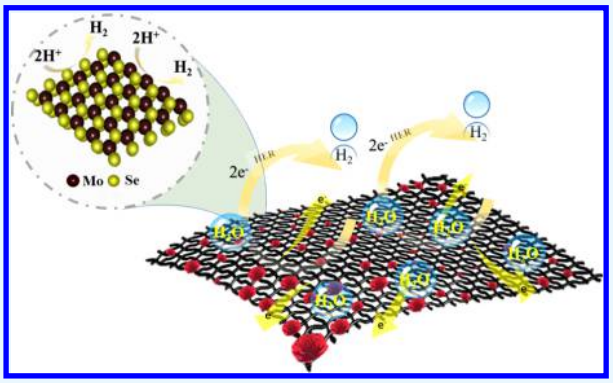

KEYWORDS: *$MoSe_2$, nanoflowers, chemical vapor deposition, electrocatalysis, hydrogen evolution reaction, XPS, in situ Raman*

1. INTRODUCTION

Two-dimensional (2D) layered materials have shown significant potential in energy field applications over the past decade owing to their excellent electrical, optical, mechanical, and (electro)chemical catalytic properties.[1] In particular, inorganic-based transition-metal dichalcogenides (TMDs), commonly represented as MX_2 (M = transition metals, and X = S, Se, Te) compounds, are emerging as a potential candidate to replace conventional catalysts in hydrogen evolution reaction (HER) and lithium-ion storage systems.[2−4] However, fundamental understanding of such materials reveals that the catalytic activity is restricted to the edge sites present in them.[5−7] It is reported that TMDs in the form of nanosheets possess maximum catalytically active sites;[2] thus, few-layered structures have been investigated extensively as (electro)catalysts.[8−11] In TMD, atomic arrangement in a single layer consists of a transition metal sandwiched between two chalcogen atoms, and a few-layered/bulk structures are formed when several single layers are stacked by weak van der Waals interlayer interaction. Thus, the resulting anisotropic structure permits top-down and bottom-up approaches to obtain mono/few-layer TMD nanosheets.[12−17] Among the wide range of TMDs, MoS_2 is comprehensively developed by various strategies and is ubiquitously considered to be an economically viable material for HER. On the other hand, selenium-based TMDs are preferred for many electronic applications because of their narrow bandgap, but they have not been studied extensively like MoS_2 for HER applications.[18,19] It has been recently predicted using density functional theory that both Mo- and Se-edge sites in $MoSe_2$ have hydrogen adsorption free energy (ΔG_H = 0.05 eV) close to zero, which can exhibit higher HER catalytic activity better than MoS_2.[20]

To date, it has been challenging to harvest $MoSe_2$ nanosheets enriched with both Mo and Se edges due to the low reactivity of selenium with molybdenum (Mo) precursors, which demands prolonged reaction time.[21−23] However, prolonged reaction time always leads to the formation of bulk structures.[24] Another approach involving the reaction of Mo precursors with rapidly vaporized selenium has guided the $MoSe_2$ growth in a perpendicular direction to the substrate. Though this approach enhances the formation of unsaturated edge sites, it predominantly encourages Mo edges.[21] Similarly, activation of $MoSe_2$ basal planes[25,26] and tailoring their morphology with preferred (either Mo or Se or both) edge-terminated structures are considered as effective approaches to enhance the density of overall active sites. However, achieving precise Mo or Se edge site is found to be dependent on the shape and morphology of formed $MoSe_2$ structures. Several

Received: May 7, 2018
Accepted: July 26, 2018
Published: July 26, 2018

DOI: 10.1021/acsami.8b07489
ACS Appl. Mater. Interfaces 2018, 10, 27771−27779

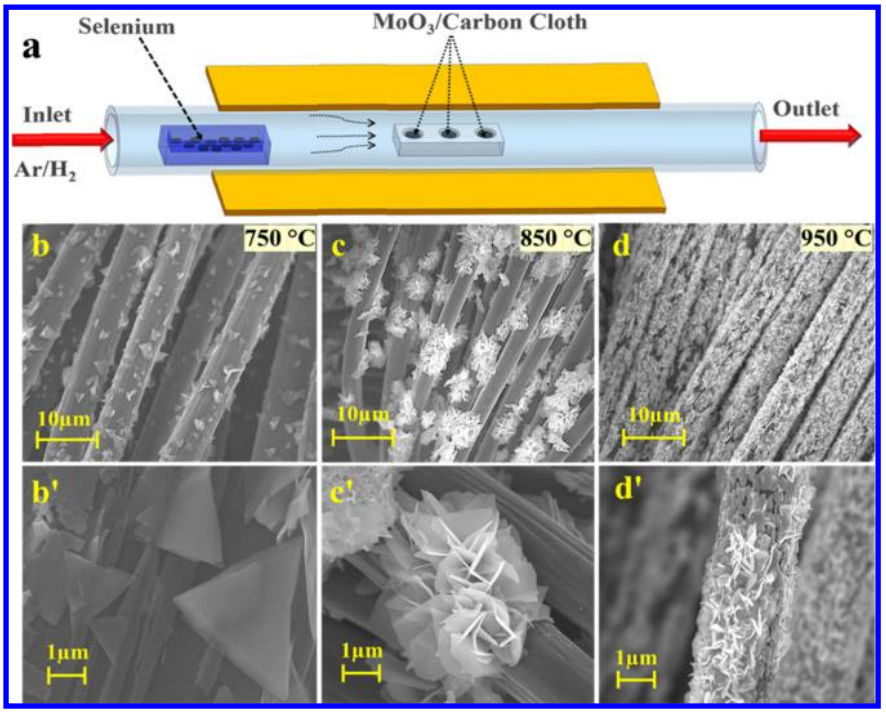

Figure 1. Growth and morphological characterization of $MoSe_2$ nanoflowers: (a) schematic representation of the experimental setup for CVD growth. (b–d) low- and (b′–d′) high-magnification SEM images of $MoSe_2$ morphology grown at (b, b′) 750 °C, (c, c′) 850 °C, (d, d′) 950 °C. Scale bars: 10 and 1 μm.

other strategies, including solvothermal,[27] colloidal,[28] and hydrothermal methods,[29,30] yield $MoSe_2$ nanosheets with heavily packed Mo edge sites that enhance the catalytic activity. On the other hand, $MoSe_2$ nanosheets synthesized directly on a conductive electrode surface alter the molecular layered structures, which increases the electronic conductivity of the layers as well as the active sites. Also, the presence of a conductive backbone network resolved the inherent charge-transfer issues during the reaction and showed a dramatic improvement in the electrocatalytic HER activity.[31−34] On the basis of these strategies, synergetic engineering of $MoSe_2$ morphologies toward abundant Mo and Se edge sites together with an efficient electronic coupling with conducting network is a potential way to obtain higher (electro)catalytic activity.

In recent years, tuning TMD morphology has been achieved with the chemical vapor deposition (CVD) process, which is a unique method to produce highly crystalline monolayer TMD nanosheets enriched with edge sites in a favorable orientation.[35] Although reports on CVD growth of $MoSe_2$ directly on a conductive surface were demonstrated with improved HER activity,[36] controlling Mo and Se edge sites precisely to increase the activity and elucidating their role in HER has not been realized so far. Here, we carried out CVD growth of $MoSe_2$ on a three-dimensional (3D) carbon cloth (CC) surface in a controlled manner by varying the parameters, such as temperature and growth time, to manipulate the surface morphology, thickness, and formation of both Mo and Se edge active sites. As grown, $MoSe_2$ on CC was subjected to detailed chemical and electrochemical characterizations to deduce the structural, electronic, and morphological features. For the electrocatalytic application, we performed HER by using typical linear polarization methods in acidic conditions. The hydrogen reduction reaction kinetics with respective different edge sites are discussed in detail with the help of a Tafel plot, exchange current density, in situ Raman, and X-ray photoelectron spectroscopy (XPS) characterization.

2. EXPERIMENTAL SECTION

2.1. Materials and Methods. CVD process: $MoSe_2$ nanoflowers were grown on a conductive CC in a furnace with a 2-inch diameter quartz tube using a CVD technique at atmospheric pressure. Initially, a CC substrate was cut into 13 mm diameter disks that were sequentially washed with acetone, iso-propanol, and distilled water for 10 min in an ultrasonic bath. An alumina boat, consisting of MoO_3 powder (99%, Sigma Aldrich) underneath the cleaned CC, was placed at the center of the reactor, i.e., high-temperature zone. A ceramic boat consisting of selenium pellets (99.9%, Sigma Aldrich) was placed in a lower-temperature zone (250−300 °C) upstream relative to the gas flow direction. Before the process, the furnace was flushed out with high-purity Ar gas for 20 min to exhaust the air. Afterward, the furnace temperature was raised to 850 °C with a ramp speed of 55 °C/min and was kept for 25 min at 850 °C by flowing a mixture of Ar (80 sccm) and H_2 (20 sccm). When the middle zone of the furnace consisting of carbon cloth and MoO_3 precursor reached 850 °C, the temperature of the Selenium boat at the upstream edge of the tube reached 250−300 °C, yielding vertically grown $MoSe_2$ nanoflowers. After the growth process, the furnace was allowed to cool down in the Ar environment.

2.2. Electrochemical Characterization. A three-electrode electrochemical cell with Ag/AgCl as a reference, Pt foil as counter, and the $MoSe_2$ grown on CC as the working electrode were used for electrochemical characterization. For the electrocatalytic purpose, 0.5 M H_2SO_4 solution was utilized, which was previously degassed with argon gas. Similarly, electrochemical impedance spectroscopy (EIS) was performed with the catalyst in 0.5 M H_2SO_4 using CH760E bipotentiostat in a frequency range of 1 MHz to 50 mHz and an amplitude of 10 mV.

2.3. In Situ Raman Experiment. In situ Raman spectroscopy was performed using an in-house built three-electrode electrochemical cell. A similar three-electrode system was set up, as described in Electrochemical Characterization. The typical recording spectrum time was 60 sec for each spectrum. To attain electrochemical

DOI: 10.1021/acsami.8b07489
ACS Appl. Mater. Interfaces 2018, 10, 27771−27779

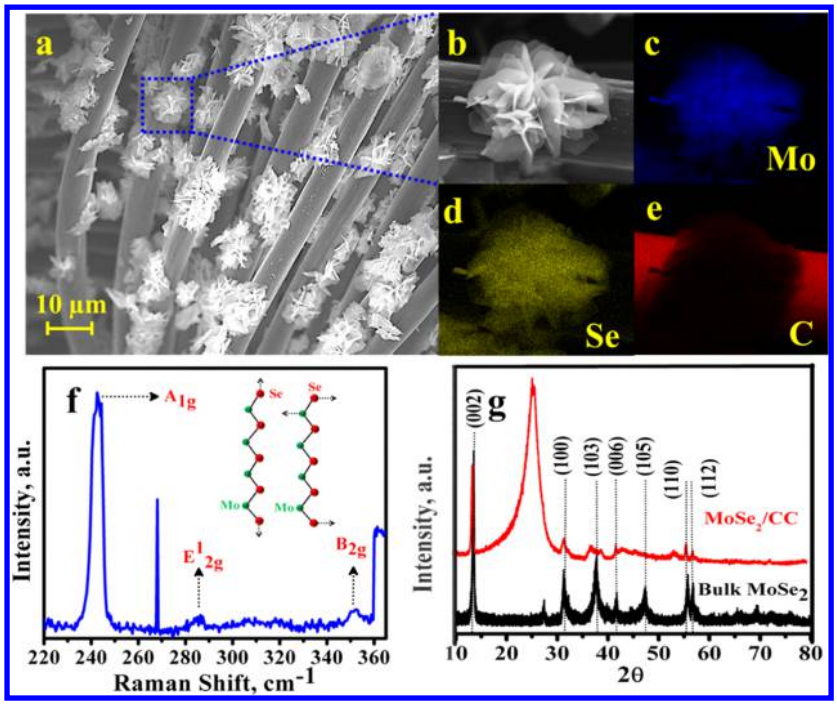

Figure 2. Characterization of $MoSe_2$ nanoflowers: (a) low-magnification SEM image of $MoSe_2$ nanoflowers. Scale bar 10 μm. (b–e) EDAX and elemental mappings of Mo, Se, and C of $MoSe_2$ nanoflowers grown on CC. (f) Raman spectra of $MoSe_2$ recorded with 532 nm green laser. (g) XRD pattern compared with bulk $MoSe_2$ (JCPDS No: 00-18-0887).

equilibrium, different potentials in 100 mV increments were applied for at least 15 min before collecting the spectrum. The band intensities used for the data analysis in this study were baseline corrected.

2.4. Characterization Methods. X-ray diffraction (XRD) patterns were recorded at a scan rate of 0.05° s^{-1} on a Rigaku Miniflex II X-ray diffractometer using Cu Kα source. Field emission electron microscopy image studies were performed on a JEOL JSM-7600 system operated with an accelerating voltage of 20 kV. X-ray photoelectron spectra (XPS) of electrode surfaces were collected using a PHI Quantera spectrophotometer, and deconvolution of spectra was performed with open source XPS peak fit 4.1 software. Raman studies were carried out on an Andor 500 series spectrometer with a 532 nm green laser excitation.

3. RESULTS AND DISCUSSION

The $MoSe_2$ nanoflowers were grown on CC by using the CVD method, as schematically illustrated in Figure 1a. In the initial setup of growth in this process, a ceramic boat, containing a MoO_3 precursor spread on the bottom side of a circular CC (13 mm diameter), was placed at the high-temperature zone, whereas a small quartz boat carrying selenium pellets was positioned at the low-temperature zone of the horizontal quartz tube. To achieve sustainable growth of $MoSe_2$ enriched with catalytic sites, CVD was carried out at different temperatures (750, 850, 950 °C). After the growth process, the morphology and composition of the as-synthesized $MoSe_2$/CC were studied by scanning electron microscopy (SEM) and energy dispersive X-ray spectroscopy (EDAX) mapping. Figure 1(b–d, low magnification) and Figure 1(b′–d′, high magnification) SEM images demonstrated that the $MoSe_2$ growth density, lateral dimensions, and morphology vary with temperature. Interestingly, it was found that the $MoSe_2$ nanosheets patterned into nanoflower morphology and distributed evenly at 850 °C, whereas incomplete growth and excessive coverage of nanosheets were observed at 750 and 950 °C. Further, the high-magnification image (Figure S1) of a nanoflower revealed the vertical orientation of several individual $MoSe_2$ nanosheets originating from a central point. The corresponding EDAX elemental mapping exposed the homogeneous distributions of Mo and Se atoms in a nanoflower on the CC, as shown in Figure 2a–e, and atomic ratio of the Mo and Se in nanoflower samples found to be 1:2 (Figure S2). During $MoSe_2$ growth, it was hypothesized that kinetics of selenization process affects the layer orientation and morphology of the nanosheets. At 750 °C, due to the low reactivity of selenium, its interaction with molybdenum precursors proceeds slowly, which provides fewer nucleation sites and leads to the formation of few-layered planar nanosheets, whereas, at 850 °C, selenium reactivity is augmented and produces many nucleation sites, which tends to form a large number of nanosheets from one core nuclei rather than enabling lateral growth. In addition, reductive nature of carbon cloth at elevated temperature enhances the reduction of MoO_3 to convert into MoO_{3-x} ($x > 1$) and limits the diffusion of selenium vapors; due to the anisotropic structure of TMDs, selenium vapors diffusion along the van der Waals gaps is expected to be much faster than diffusion across the layers, which provides vertical orientation for nanoflowers.[21] The vertically aligned discrete $MoSe_2$ nanosheets coalesce to reduce the surface energy and convert into a nanoflower morphology. On the other hand, at 950 °C, the concentrations of both selenium vapors and MoO_{3-x} ($x > 1$) increase drastically, which lead to an uncontrollable reaction between them and eventually form excessive $MoSe_2$ nanosheets, which cover the whole carbon cloth.

To gain further evidence, we performed Raman spectroscopic analysis on $MoSe_2$/CC samples using a 532 nm laser source, as shown in Figure 2f. The $MoSe_2$/CC nanoflowers showed the typical Raman vibration modes, such as in-plane ($^1E_{2g}$) and out-of-plane (A_{1g}) modes, at 287 and 242 cm^{-1},

DOI: 10.1021/acsami.8b07489
ACS Appl. Mater. Interfaces 2018, 10, 27771–27779

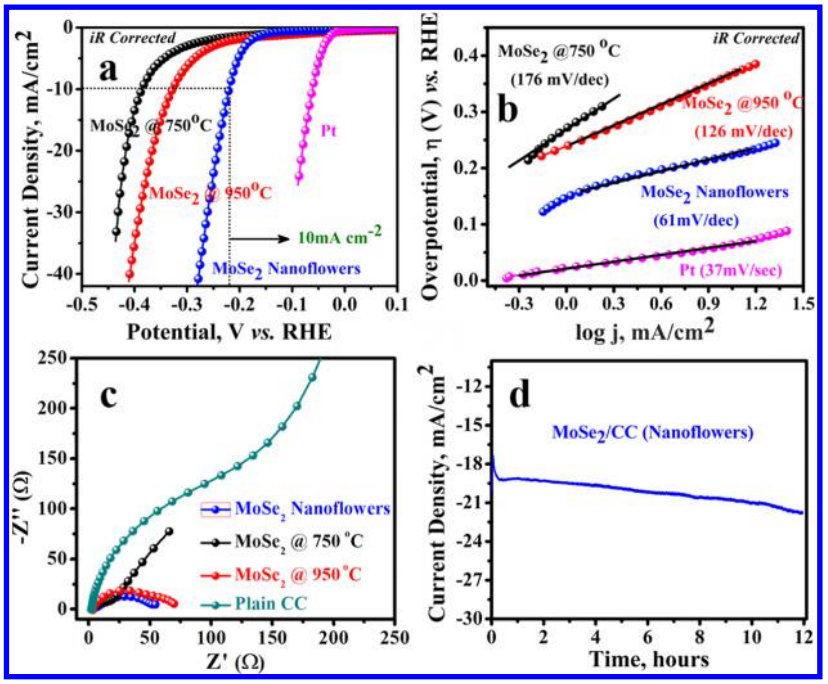

Figure 3. Electrocatalytic hydrogen evolution on $MoSe_2$ nanoflowers: (a) HER polarization curve on $MoSe_2$ nanoflowers (blue) compared with $MoSe_2$ grown at 750 °C (black), 950 °C (red), and benchmark Pt/C catalyst (magenta). Scan rate: 1 mV/s. (b) Tafel plot (η vs log j, mA/cm^2). (c) EIS Nyquist plot of $MoSe_2$ nanoflowers (blue) compared with $MoSe_2$ grown at 750 °C (black), 950 °C (Red). Alternating current frequency range: 1 MHz to 100 mHz. Amplitude: 10 mV. (d) Stability of $MoSe_2$ catalytic activity against HER (chronoamperometry performed at overpotential (η) of 250 mV).

respectively. For comparison, Raman spectra of samples grown at different temperatures were taken, which showed similar spectral features with slight red-shift in frequency values (Figure S3). The obtained Raman spectrum of $MoSe_2$ nanoflowers is in agreement with previous studies in terms of the $^1E_{2g}$ peak shift to the higher wavenumber and the A_{1g} peak moving to the lower number.[37,38] It is well understood from theoretical studies that the A_{1g} peak preferentially originates from the edge-terminated structures, whereas the $^1E_{2g}$ peak arises due to the basal plane, and the ratio of the relative intensity between these two modes provides information about the density of the active sites.[39] In our work, the intensity of the $^1E_{2g}$ peak is significantly smaller (about 10%) compared to the A_{1g} peak, indicating that the $MoSe_2$ nanoflowers are supplemented with a substantial amount of active edge sites. In addition to these Raman characteristics, an extra peak around 355 cm^{-1} was pronounced in $MoSe_2$ nanoflower samples. It is noteworthy to mention that this peak (assigned as a B_{2g} vibrational mode) is inactive in monolayer and bulk but active in a few layers due to the breakdown of translation symmetry.[40,41] Hence, the appearance of the B_{2g} vibrational mode in Raman spectra further confirms the flower type of morphology associated with the few layers of nanosheets. Figure 2g shows the X-ray diffraction (XRD) pattern of $MoSe_2$ nanoflowers along with the bulk $MoSe_2$ sample. The $MoSe_2$ nanoflowers exhibit a strong diffraction pattern at 2θ = 13.51° that corresponds to the (002) plane, which specified the 2H symmetrical hexagonal phase of $MoSe_2$/CC. However, other characteristic peaks at 2θ = 31.29, 37.76, 41.50, 47.40, 56.14, and 56.89° associated with the (100), (103), (006), (105), (110), and (112) planes, respectively, exhibit considerably lower intensities in $MoSe_2$ nanoflowers than the bulk sample. This observation demonstrates that $MoSe_2$ nanoflowers preferably grow in the z-axis (002) direction, which usually indicates the formation of vertically oriented nanosheets and the presence of more unsaturated sites.[42] In addition, XRD patterns of $MoSe_2$ grown at different temperatures (Figure S4) indicate that the relative intensity of the (002) plane peak is increased with temperature from 750 to 950 °C. From microscopic and spectroscopic characterizations, it can be concluded that vertically aligned $MoSe_2$ nanoflowers grown on CC by the vapor diffusion method have abundant active edge sites and can be expected to show higher electrocatalytic activity.

To evaluate the electrocatalytic activity of $MoSe_2$/CC, HER was performed in acidic conditions (0.5 M H_2SO_4) using linear sweep voltammetry with a conventional three-electrode setup at a scan rate of 1 mV/s. Figure 3a shows the comparative voltammograms of $MoSe_2$ grown at different temperatures along with a benchmark platinum (Pt) catalyst. During the cathodic sweep, $MoSe_2$ nanoflowers showed minimal onset potential for hydrogen reduction (η = 170 mV vs reversible hydrogen electrode (RHE)) followed by a sharp rise in current, which denotes a high catalytic nature in HER, whereas, $MoSe_2$ grown at 750 and 950 °C displayed the onset potential and HER catalytic current at > 250 mV vs RHE. The reduced overpotential for hydrogen reduction on $MoSe_2$ nanoflowers was likely due to the vertical orientation of $MoSe_2$ nanosheets, which decreases the hydrogen adsorption energy on catalytically active edge sites.[32] To further corroborate the catalytic activity, we performed a Tafel analysis on the obtained polarization curves with *iR*-correction, as demonstrated in Figure 3b. It was found that $MoSe_2$ nanoflowers exhibited a Tafel slope value of 61 mV/dec, which is very low compared to other samples grown at 750 °C (176 mV/dec) and 950 °C (126 mV/dec). Naturally, Pt displayed (37 mV/dec) the lowest Tafel slope value among all of the electrocatalysts studied for HER.

DOI: 10.1021/acsami.8b07489
ACS Appl. Mater. Interfaces 2018, 10, 27771−27779

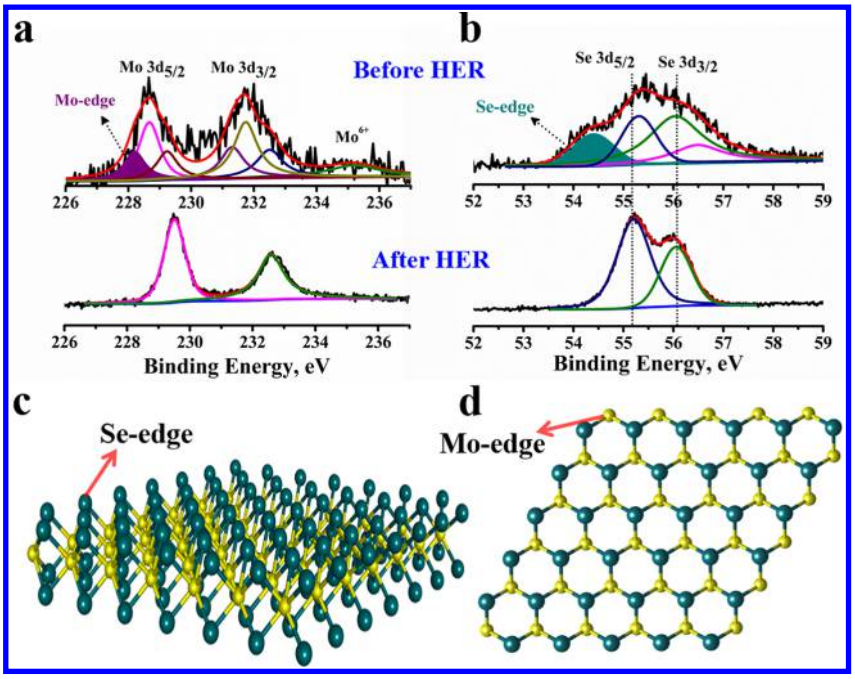

Figure 4. Hydrogen adsorption active sites on $MoSe_2$ nanoflowers: XPS spectrum of (a) Mo 3d spectra (b) Se 3d spectra (deconvolution of spectra was performed with open source XPS peak fit 4.1 software). (c, d) Structural representation of $MoSe_2$ nanoflowers in horizontal and top view, respectively. (c) and (d) were made using Materials Project Online software (database version 3.0.0 powered by Pymatgen version 2018.6.11).[47,48] (c) and (d), and the table of contents graphic were made using VESTA 3.4.0.[49]

Similarly, the exchange current density (j_o) was calculated from the extrapolation of *X*-axis in the Tafel plot, and it was found that $MoSe_2$/CC (0.85 mA/cm^2) nanoflowers show higher j_o compared to the samples grown at 750 °C (0.24 mA/cm^2) and 950 °C (0.18 mA/cm^2). In addition, the enhancement of HER kinetics was confirmed from the overpotential measured at 10 mA/cm^2 HER current, and it was found that nanoflower samples require only η = 220 mV, whereas $MoSe_2$ grown at 750 °C and 950 °C need >350 mV. From the Tafel and exchange current analyses, it is evident that $MoSe_2$ with a nanoflower structure exhibits enhanced HER kinetics compared to other samples and previous reports in the literature (Table S1). Although numerous reports exist on HER using TMDs as electrocatalysts, elucidating the responsible mechanism has remained indecisive. Previous reports explained that hydrogen reduction on any surface occurs either by hydrogen−hydrogen atom (Volmer−Tafel) or hydrogen ion−hydrogen recombination (Volmer−Heyrovsky), which can be elucidated from the Tafel slope values. If the Tafel slope is below 40 mV/dec, HER takes place via Volmer−Tafel and of above 40 mV/dec, it follows the Volmer−Heyrovsky mechanism.[43,44] This suggests that the HER on $MoSe_2$/CC nanoflowers undergoes two-electron transfer reductions, i.e., the Volmer−Heyrovsky type of mechanism and electrolytic desorption process, which could be the rate-deciding step. The improvement of the catalytic property of nanoflowers can be likely due to more coverage of hydrogen ions on edge sites as well as the efficient charge transportation between $MoSe_2$ layers and the CC conducting network during electrocatalysis.[32]

To further verify the enhancement in $MoSe_2$/CC nanoflower charge-transport activity, we performed electrochemical impedance spectroscopy (EIS). Figure 3c demonstrates Nyquist plots of $MoSe_2$/CC nanoflowers measured at open circuit potential, which is compared with other samples and blank CC. In EIS, nanoflower samples exhibited charge-transfer resistance (R_{ct}) of 60 Ω, which is lower than for the $MoSe_2$ grown at 750 °C (125 Ω), 950 °C (90 Ω), and blank CC (150 Ω). Obtaining higher impedance values on 750 °C (Figure S5) and 950 °C samples can be ascribed to the formation of incomplete and complete coverage of $MoSe_2$ nanosheets on CC fibers, respectively. The complete coverage of $MoSe_2$ on CC having more active sites blocks the electron transportation due to higher density, which is in agreement with earlier reports.[34] This evaluation clearly validates the reason behind the low HER kinetic current, the decrease in exchange current density, and the higher Tafel slope gained on 950 °C $MoSe_2$ samples during polarization experiments. On the other hand, major reduction in the R_{ct} value on $MoSe_2$ nanoflower morphology can be attributed to its vertical orientation on CC, which creates more charge interaction between them and reduces the free energy associated with the electron-hopping process, ending with efficient charge transport.[32] In addition to $MoSe_2$ nanoflowers having better catalytic property, their enduring stability against hydrogen production is of vital importance in industrial level catalyst development. Indeed, TMDs directly grown on a carbon substrate efficiently stabilize their structure when compared to other synthesis methods and have a significant impact on their stability during electrocatalysis.[33,45] This effect is more pronounced when TMDs are aligned in the vertical direction, which creates a strong interaction with the carbon surface; hence, our $MoSe_2$ nanoflowers on CC can be expected to show remarkable stability during HER. To show such feasibility, the $MoSe_2$/CC surface was exposed to an acidic solution with a supply of constant overpotential (η = 250 mV) over a long period of time. As shown in Figure 3d, an initial current (18 mA/cm^2) at 250 mV potential remains stable for a specified period (~9 h); afterward, it started to increase and reached 22 mA/cm^2 at 12 h (~20% higher). The increment is rational due

DOI: 10.1021/acsami.8b07489
ACS Appl. Mater. Interfaces 2018, 10, 27771−27779

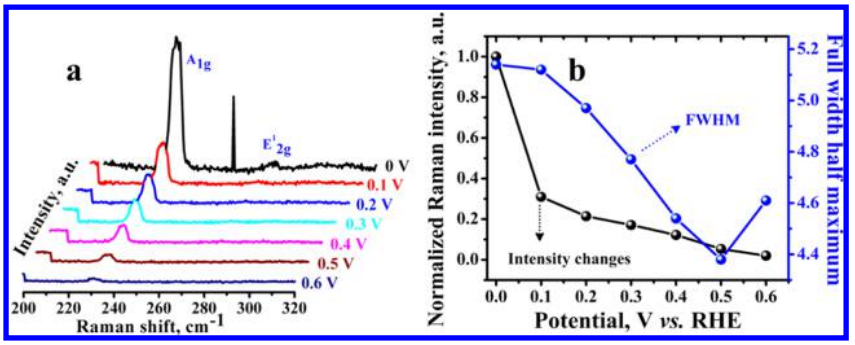

Figure 5. In situ Raman monitoring of HER on $MoSe_2$ nanoflowers: (a) spectrum recorded at different overpotentials (η) from 0 to 0.6 V (532 nm green laser). (b) Variation in Raman intensity (baseline corrected) and full width half maximum with respect to different overpotentials.

to the elimination of surface impurities and renewal of fresh active sites on a prolonged operation time. This excellent stability against hydrogen production shows the potential utility of $MoSe_2$ nanoflowers for an efficient water electrolysis process.

Here, we have shown CVD-grown $MoSe_2$ nanoflowers on CC with high catalytic active edges because of vertically oriented structure that provide promising HER activity. A further understanding of $MoSe_2$ nanoflower active sites that influence the catalytic activity in HER will be helpful to engineer a suitable catalyst in the future. In addition to the edge reliant reactivity, the electronic behavior of TMDs is largely influenced by heterogeneity on the surface, i.e., edge planes are metallic whereas basal planes are semiconducting in nature as evidenced from both theoretical and experimental studies.[46] The interplay between the edge sites and electronic structure in TMDs are well demonstrated, and its structure reconstruction upon hydrogen adsorption was studied in detail.

For understanding hydrogen adsorption sites in $MoSe_2$/CC nanoflowers, we performed detailed X-ray photoelectron spectroscopy (XPS) investigation before and after the HER process. Figure 4a illustrates that the Mo 3d core-levels of $MoSe_2$ before and after HER show a typical splitting of the $MoSe_2$ doublet peak that corresponds to the Mo $3d_{3/2}$ and $3d_{5/2}$ orbitals. The Mo 3d spectra of pristine $MoSe_2$ (before HER) show lower binding energy values with a broadened peak which is distinct from the reported bulk Mo 3d XPS spectrum,[50] indicating the existence of different Mo atomic structures. Further, the deconvoluted spectra of Mo $3d_{5/2}$ revealed that it has three peaks, which include two predominant peaks at 229.2, 228.8 eV and a smaller one at 228.3 eV. Previously, it has been described that binding energies corresponding to the metallic edges always transpired at lower values and was well demonstrated for MoS_2 on gold substrates, exfoliated MoS_2 and $MoSe_2$ layers.[51,52] Hence, the lower binding energy peak observed in the Mo $3d_{5/2}$ spectrum indicates the existence of unsaturated Mo-edge planes in $MoSe_2$ nanoflower samples, which was further validated by the presence of ~0.5 eV difference in between two predominant peaks of Mo $3d_{5/2}$. The other doublet peak of higher binding energies at 231.4 and 235.0 eV corresponds to the Mo $3d_{3/2}$ and Mo^{6+}, respectively, as illustrated in Figure 4a. Similarly, the Se 3d spectrum of the $MoSe_2$/CC occurs with significant peak broadening, as shown in Figure 4b, and the fitting affirms the presence of two sets of doublet peaks. The peaks obtained at 55.34 and 56.04 eV correspond to the typical Se $3d_{3/2}$ and Se $3d_{5/2}$ orbitals, respectively. Similar to the Mo 3d spectrum, the Se 3d spectra have a lower binding energy (54.39 eV) peak, which is certainly due to the unsaturated Se^{2-} and terminal Se_2^{2-} atoms. Theoretical studies of TMD flake structure predicted that the inverted triangle shape could accommodate both Se- and Mo-rich types of catalytic active edge sites simultaneously, which is difficult to achieve in other morphologies.[53] XPS studies are in good agreement with morphologies observed through SEM images, showing that the vertically aligned 2D $MoSe_2$ nanoflower's petals exhibit an inverted triangular shape (Figure S6).

Hence, it is safe to conclude that nanoflowers consist of both the unsaturated Se and Mo atoms all over the edge site, as schematically illustrated in Figure 4c,d. In addition to the edge plane confirmation, the lower binding energies suggest the presence of more negative charges on the terminal edge sites, which can share the electrons easily with electrophilic atoms, like hydrogen (in the HER case). Previously, XPS investigations of hydrogen adsorption on the edge planes of MoS_2 under reactive circumstances indicated the intensity variations among the peaks during the reaction due to the edge planes reactivity; however, no visible changes in the binding energy values were observed in the spectrum.[54] Indeed, we found that the intensity of lower binding energy peaks on both Mo 3d and Se 3d vanished, and significant variation in the shape of the peak (from broader to sharper after HER process) was observed, as shown in Figure 4a,b. This observation can be explained as adsorption of hydrogen ions on edge sites significantly change the $MoSe_2$ electronic conductivity from metallic to semimetallic and the corresponding peak binding energy value shifts to higher values. This observation is in line with previous results where a reduction in XANES peak intensity was observed on terminal disulfide ligands of MoS_x materials upon hydrogen adsorption.[55]

To understand surface/interface reactions during the electrochemical process, we performed in situ Raman spectroscopy containing a specially designed liquid immersion objective lens, which will drastically reduce the refractive index mismatch in the optical path at the air/electrolyte interface. Thus, it provides a significant improvement in the sensitivity and spatial resolution of the Raman signal. Figure 5a shows in situ Raman spectra recorded at different hydrogen evolution overpotential regions, viz, from 0 to 0.6 V vs RHE. In this case, no change in the position and intensity of Raman vibration bands was seen when the sample was in contact with an acidic solution, which confirms the stability of $MoSe_2$ structures on the 3D carbon surface. As the potential swept toward a cathodic direction, the $^1E_{2g}$ peak completely attenuated and the intensity of the A_{1g} peak gradually decreased along with peak broadening. Further increment of cathodic potential, the

DOI: 10.1021/acsami.8b07489
ACS Appl. Mater. Interfaces 2018, 10, 27771−27779

intensity of A_{1g} peak completely reduced, which can be explained as follows. It has been well demonstrated that the A_{1g} phonon involves selenium atomic vibration opposite from the *c*-axis and has a higher tendency to interact with reactant molecules.[56] In the HER case, the increase in the cathodic potential induces the adsorption of more H^+ ions on the $MoSe_2$ edge sites, which persuades the reduction in peak intensity. Also, during hydrogen interaction with the edge sites, the charge transfer between the scattered phonon−electrons results in intensity reduction and peak broadening (Figure 5b). This observation is consistent with earlier reports that Raman intensities of amorphous MoS_x terminal edges were attenuated upon interaction with hydrogen,[57] and reports indicated the edge site's participation during HER. The low Tafel slope value and higher exchange current density gained from $MoSe_2$/CC nanoflowers were attributed to the dual (Mo- and Se-rich) active sites present in them and exemplified with XPS and in situ Raman characterizations.

4. CONCLUSIONS

In summary, we have successfully demonstrated the direct growth of $MoSe_2$ nanoflower structures on a CC surface, enriched with active Mo and Se edge sites, by using a CVD technique. A combination of spectroscopic and microscopic studies revealed that the $MoSe_2$ nanoflowers were constructed by the amalgamation of a few layers of nanosheets in perpendicular to the substrate with all the unsaturated edge sites exposed. As a result, the $MoSe_2$/CC electrode showed enhanced electrocatalytic activity on hydrogen reduction, including a lower Tafel slope and a higher exchange of current density. Further, impedance results proved that the synergistic effect of the 3D carbon surface and 2D $MoSe_2$ nanosheets increases the electron-hopping process by reducing the charge-transfer resistance across the electrode−electrolyte interface. In situ Raman and XPS studies provide detailed evidence on hydrogen adsorption on dual active sites viz., Mo and Se edges present in $MoSe_2$/CC. The present work proposed an efficient route to increase the active catalytic sites and the electrical conductivity of metal dichalcogenides-based HER electrodes, enabling their potential to replace contemporary electrocatalysts for the HER process.

■ ASSOCIATED CONTENT

Supporting Information

The Supporting Information is available free of charge on the ACS Publications website at DOI: 10.1021/acsami.8b07489.

Further morphological and structural characterization; comparison of $MoSe_2$ nanoflower HER activity with $MoSe_2$ grown by other methods (PDF)

■ AUTHOR INFORMATION

Corresponding Author

*E-mail: leela.arava@wayne.edu.

ORCID

Naresh Kumar Thangavel: 0000-0002-6604-0211

Leela Mohana Reddy Arava: 0000-0001-6685-6061

Author Contributions

N.M., N.K.T., and L.M.R.A. conceived and designed the experiments. N.K.T. performed all of the experimental work with N.M. The experimental data were analyzed by N.K.T. with N.M. and L.M.R.A. All of the authors contributed in writing and editing the manuscript.

Notes

The authors declare no competing financial interest.

■ ACKNOWLEDGMENTS

This article was supported in part by the NSF Division of Chemical, Bioengineering, Environmental, and Transport Systems (CBET: 1748363) and ACS Petroleum Research Fund (ACSPRF: 57647-DNI10).

■ REFERENCES

(1) Kuila, T.; Bose, S.; Mishra, A. K.; Khanra, P.; Kim, N. H.; Lee, J. H. Chemical Functionalization of Graphene and Its Applications. *Prog. Mater. Sci.* **2012**, *57*, 1061−1105.

(2) Chhowalla, M.; Shin, H. S.; Eda, G.; Li, L. J.; Loh, K. P.; Zhang, H. The Chemistry of Two-Dimensional Layered Transition Metal Dichalcogenide Nanosheets. *Nat. Chem.* **2013**, *5*, 263−275.

(3) Benck, J. D.; Hellstern, T. R.; Kibsgaard, J.; Chakthranont, P.; Jaramillo, T. F. Catalyzing the Hydrogen Evolution Reaction (HER) with Molybdenum Sulfide Nanomaterials. *ACS Catal.* **2014**, *4*, 3957−3971.

(4) Angelici, R. J. Heterogeneous Catalysis of the Hydrodesulfurization of Thiophenes in Petroleum: An Organometallic Perspective of the Mechanism. *Acc. Chem. Res.* **1988**, *21*, 387−394.

(5) Chianelli, R. Fundamental Studies of Transition Metal Sulfide Hydrodesulfurization Catalysts. *Catal. Rev.* **1984**, *26*, 361−393.

(6) Jaramillo, T. F.; Jørgensen, K. P.; Bonde, J.; Nielsen, J. H.; Horch, S.; Chorkendorff, I. Identification of Active Edge Sites for Electrochemical H_2 Evolution from MoS_2 Nanocatalysts. *Science* **2007**, *317*, 100−102.

(7) Byskov, L. S.; Nørskov, J. K.; Clausen, B. S.; Topsøe, H. DFT Calculations of Unpromoted and Promoted MoS_2-Based Hydrodesulfurization Catalysts. *J. Catal.* **1999**, *187*, 109−122.

(8) Lee, Y. H.; Zhang, X. Q.; Zhang, W.; Chang, M. T.; Lin, C. T.; Chang, K. D.; Yu, Y. C.; Wang, J. T. W.; Chang, C. S.; Li, L. J.; et al. Synthesis of Large-Area MoS_2 Atomic Layers with Chemical Vapor Deposition. *Adv. Mater.* **2012**, *24*, 2320−2325.

(9) Liu, K. K.; Zhang, W.; Lee, Y. H.; Lin, Y. C.; Chang, M. T.; Su, C. Y.; Chang, C. S.; Li, H.; Shi, Y.; Zhang, H.; et al. Growth of Large-Area and Highly Crystalline MoS_2 Thin Layers on Insulating Substrates. *Nano Lett.* **2012**, *12*, 1538−1544.

(10) Xia, J.; Huang, X.; Liu, L. Z.; Wang, M.; Wang, L.; Huang, B.; Zhu, D. D.; Li, J. J.; Gu, C. Z.; Meng, X.-M. CVD Synthesis of Large-Area, Highly Crystalline $MoSe_2$ Atomic Layers on Diverse Substrates and Application to Photodetectors. *Nanoscale* **2014**, *6*, 8949−8955.

(11) Naresh Kumar, T.; Chandrasekaran, N.; Lakshminarasimha Phani, K. Structural and Electronic Modification of MoS_2 Nanosheets Using S-Doped Carbon for Efficient Electrocatalysis of the Hydrogen Evolution Reaction. *Chem. Commun.* **2015**, *51*, 5052−5055.

(12) Eda, G.; Yamaguchi, H.; Voiry, D.; Fujita, T.; Chen, M.; Chhowalla, M. Photoluminescence from Chemically Exfoliated MoS2. *Nano Lett.* **2011**, *11*, 5111−5116.

(13) Li, H.; Wu, J.; Yin, Z.; Zhang, H. Preparation and Applications of Mechanically Exfoliated Single-Layer and Multilayer MoS_2 and WSe_2 Nanosheets. *Acc. Chem. Res.* **2014**, *47*, 1067−1075.

(14) Lukowski, M. A.; Daniel, A. S.; Meng, F.; Forticaux, A.; Li, L.; Jin, S. Enhanced Hydrogen Evolution Catalysis from Chemically Exfoliated Metallic MoS_2 Nanosheets. *J. Am. Chem. Soc.* **2013**, *135*, 10274−10277.

(15) Chua, C. K.; Loo, A. H.; Pumera, M. Top-Down and Bottom-up Approaches in Engineering 1T Phase Molybdenum Disulfide (MoS_2): Towards Highly Catalytically Active Materials. *Chem. - Eur. J.* **2016**, *22*, 14336−14341.

(16) Li, X.; Zhu, H. Two-Dimensional MoS_2: Properties, Preparation, and Applications. *J. Materiomics* **2015**, *1*, 33−44.

DOI: 10.1021/acsami.8b07489
ACS Appl. Mater. Interfaces 2018, 10, 27771−27779

(17) Shi, Y.; Li, H.; Li, L.-J. Recent Advances in Controlled Synthesis of Two-Dimensional Transition Metal Dichalcogenides Via Vapour Deposition Techniques. *Chem. Soc. Rev.* **2015**, *44*, 2744−2756.
(18) Liu, Y.; Stradins, P.; Wei, S.-H. Van der Waals Metal-Semiconductor Junction: Weak Fermi Level Pinning Enables Effective Tuning of Schottky Barrier. *Sci. Adv.* **2016**, *2*, e1600069−e1600076.
(19) Eftekhari, A. Molybdenum Diselenide ($MoSe_2$) for Energy Storage, Catalysis, and Optoelectronics. *Appl. Mater. Today* **2017**, *8*, 1−17.
(20) Tsai, C.; Chan, K.; Abild-Pedersen, F.; Norskov, J. K. Active Edge Sites in $MoSe_2$ and WSe_2 Catalysts for the Hydrogen Evolution Reaction: A Density Functional Study. *Phys. Chem. Chem. Phys* **2014**, *16*, 13156−13164.
(21) Kong, D.; Wang, H.; Cha, J. J.; Pasta, M.; Koski, K. J.; Yao, J.; Cui, Y. Synthesis of MoS_2 and $MoSe_2$ Films with Vertically Aligned Layers. *Nano Lett.* **2013**, *13*, 1341−1347.
(22) Lu, X.; Utama, M. I. B.; Lin, J.; Gong, X.; Zhang, J.; Zhao, Y.; Pantelides, S. T.; Wang, J.; Dong, Z.; Liu, Z.; Zhou, W.; Xiong, Q. Large-Area Synthesis of Monolayer and Few-Layer $MoSe_2$ Films on SiO_2 Substrates. *Nano Lett.* **2014**, *14*, 2419−2425.
(23) Tsirlina, T.; Feldman, Y.; Homyonfer, M.; Sloan, J.; Hutchison, J. L.; Tenne, R. Synthesis and Characterization of Inorganic Fullerene-Like WSe_2 Material. *Fullerene Sci. Technol.* **1998**, *6*, 157−165.
(24) Wu, Z.; Guoan, T.; Xufeng, W.; Tingsong, H.; Rui, W.; Wanlin, G. Large-Area Synthesis and Photoelectric Properties of Few-Layer $MoSe_2$ on Molybdenum Foils. *Nanotechnology* **2018**, *29*, No. 125605.
(25) Lin, S.-H.; Kuo, J.-L. Activating and Tuning Basal Planes of MoO_2, MoS_2, and $MoSe_2$ for Hydrogen Evolution Reaction. *Phys. Chem. Chem. Phys.* **2015**, *17*, 29305−29310.
(26) Gao, D.; Xia, B.; Zhu, C.; Du, Y.; Xi, P.; Xue, D.; Ding, J.; Wang, J. Activation of the $MoSe_2$ Basal Plane and Se-Edge by B Doping for Enhanced Hydrogen Evolution. *J. Mater. Chem. A.* **2018**, *6*, 510−515.
(27) Jiang, M.; Zhang, J.; Wu, M.; Jian, W.; Xue, H.; Ng, T.-W.; Lee, C.-S.; Xu, J. Synthesis of 1T-$MoSe_2$ ultrathin Nanosheets with an Expanded Interlayer Spacing of 1.17 nm for Efficient Hydrogen Evolution Reaction. *J. Mater. Chem. A* **2016**, *4*, 14949−14953.
(28) Sun, D.; Feng, S.; Terrones, M.; Schaak, R. Formation and Interlayer Decoupling of Colloidal $MoSe_2$ Nanoflowers. *Chem. Mater.* **2015**, *27*, 3167−3175.
(29) Tang, H.; Dou, K.; Kaun, C.-C.; Kuang, Q.; Yang, S. $MoSe_2$ nanosheets and Their Graphene Hybrids: Synthesis, Characterization and Hydrogen Evolution Reaction Studies. *J. Mater. Chem. A* **2014**, *2*, 360−364.
(30) Xu, S.; Lei, Z.; Wu, P. Facile Preparation of 3D MoS_2/$MoSe_2$ nanosheet−Graphene Networks as Efficient Electrocatalysts for the Hydrogen Evolution Reaction. *J. Mater. Chem. A* **2015**, *3*, 16337−16347.
(31) Tsai, C.; Abild-Pedersen, F.; Nørskov, J. K. Tuning the MoS_2 Edge-Site Activity for Hydrogen Evolution Via Support Interactions. *Nano Lett.* **2014**, *14*, 1381−1387.
(32) Li, H.; Yu, K.; Li, C.; Tang, Z.; Guo, B.; Lei, X.; Fu, H.; Zhu, Z. Charge-Transfer Induced High Efficient Hydrogen Evolution of MoS_2/Graphene Cocatalyst. *Sci. Rep.* **2015**, *5*, No. 18730.
(33) Qu, B.; Yu, X.; Chen, Y.; Zhu, C.; Li, C.; Yin, Z.; Zhang, X. Ultrathin $MoSe_2$ Nanosheets Decorated on Carbon Fiber Cloth as Binder-Free and High-Performance Electrocatalyst for Hydrogen Evolution. *ACS Appl. Mater. Interfaces* **2015**, *7*, 14170−14715.
(34) Liu, Y.; Ren, L.; Zhang, Z.; Qi, X.; Li, H.; Zhong, J. 3D Binder-Free $MoSe_2$ Nanosheets/Carbon Cloth Electrodes for Efficient and Stable Hydrogen Evolution Prepared by Simple Electrophoresis Deposition Strategy. *Sci. Rep.* **2016**, *6*, No. 22516.
(35) Ji, Q.; Zhang, Y.; Shi, J.; Sun, J.; Zhang, Y.; Liu, Z. Morphological Engineering of CVD-Grown Transition Metal Dichalcogenides for Efficient Electrochemical Hydrogen Evolution. *Adv. Mater.* **2016**, *28*, 6207−6212.
(36) Chen, X.; Wang, Z.; Qiu, Y.; Zhang, J.; Liu, G.; Zheng, W.; Feng, W.; Cao, W.; Hu, P.; Hu, W. Controlled Growth of Vertical 3D $MoS_{2(1-x)}$ Se_{2x} Nanosheets for an Efficient and Stable Hydrogen Evolution Reaction. *J. Mater. Chem. A* **2016**, *4*, 18060−18066.
(37) Sun, D.; Feng, S.; Terrones, M.; Schaak, R. E. Formation and Interlayer Decoupling of Colloidal $MoSe_2$ Nanoflowers. *Chem. Mater.* **2015**, *27*, 3167−3175.
(38) Shaw, J. C.; Zhou, H.; Chen, Y.; Weiss, N. O.; Liu, Y.; Huang, Y.; Duan, X. Chemical Vapor Deposition Growth of Monolayer $MoSe_2$ Nanosheets. *Nano Res.* **2014**, *7*, 511−517.
(39) Gao, M. R.; Chan, M. K.; Sun, Y. Edge-Terminated Molybdenum Disulfide with a 9.4 Å Interlayer Spacing for Electrochemical Hydrogen Production. *Nat. Commun.* **2015**, *6*, No. 7493.
(40) Tonndorf, P.; Schmidt, R.; Böttger, P.; Zhang, X.; Börner, J.; Liebig, A.; Albrecht, M.; Kloc, C.; Gordan, O.; Zahn, D. R.; et al. Photoluminescence Emission and Raman Response of Monolayer MoS_2, $MoSe_2$, and WSe_2. *Opt. Express* **2013**, *21*, 4908−4916.
(41) Terrones, H.; Del Corro, E.; Feng, S.; Poumirol, J.; Rhodes, D.; Smirnov, D.; Pradhan, N.; Lin, Z.; Nguyen, M.; Elias, A.; et al. New First Order Raman-Active Modes in Few Layered Transition Metal Dichalcogenides. *Sci. Rep.* **2014**, *4*, No. 4215.
(42) Jung, C.; Kim, S. M.; Moon, H.; Han, G.; Kwon, J.; Hong, Y. K.; Omkaram, I.; Yoon, Y.; Kim, S.; Park, J. Highly Crystalline Cvd-Grown Multilayer $MoSe_2$ Thin Film Transistor for Fast Photo-detector. *Sci. Rep.* **2015**, *5*, No. 15313.
(43) Kibler, L. A. Hydrogen Electrocatalysis. *Chem. Phys. Chem.* **2006**, *7*, 985−991.
(44) Zheng, Y.; Jiao, Y.; Jaroniec, M.; Qiao, S. Z. Advancing the Electrochemistry of the Hydrogen-Evolution Reaction through Combining Experiment and Theory. *Angew. Chem., Int. Ed.* **2015**, *54*, 52−65.
(45) Youn, D. H.; Han, S.; Kim, J. Y.; Kim, J. Y.; Park, H.; Choi, S. H.; Lee, J. S. Highly Active and Stable Hydrogen Evolution Electrocatalysts Based on Molybdenum Compounds on Carbon Nanotube−Graphene Hybrid Support. *ACS Nano* **2014**, *8*, 5164−5173.
(46) Lin, Y. C.; Dumcenco, D. O.; Huang, Y.-S.; Suenaga, K. Atomic Mechanism of the Semiconducting-to-Metallic Phase Transition in Single-Layered MoS_2. *Nat. Nanotechnol.* **2014**, *9*, 391−396.
(47) Jain, A.; Ong, S. P.; Hautier, G.; Chen, W.; Richards, W. D.; Dacek, S.; Cholia, S.; Gunter, D.; Skinner, D.; Ceder, G.; Persson, K. A. Commentary: The Materials Project: A Materials Genome Approach to Accelerating Materials Innovation. *APL Mater.* **2013**, *1*, 011002−011013.
(48) Ong, S. P.; Richards, W. D.; Jain, A.; Hautier, G.; Kocher, M.; Cholia, S.; Gunter, D.; Chevrier, V. L.; Persson, K.; Ceder, G. Python Materials Genomics (pymatgen): A Robust, Open-Source Python Library for Materials Analysis. *Comput. Mater. Sci.* **2013**, *68*, 314−319.
(49) Momma, K.; Izumi, F. VESTA 3 for Three-dimensional Visualization of Crystal, Volumetric and Morphology Data. *J. Appl. Crystallogr.* **2011**, *44*, 1272−1276.
(50) Abada, S.; Marlair, G.; Lecocq, A.; Petit, M.; Sauvant-Moynot, V.; Huet, F. Safety Focused Modeling of Lithium-Ion Batteries: A Review. *J. Power Sources* **2016**, *306*, 178−192.
(51) Naz, M.; Hallam, T.; Berner, N. C.; McEvoy, N.; Gatensby, R.; McManus, J. B.; Akhter, Z.; Duesberg, G. S. A New 2H-2H′/1T Cophase in Polycrystalline MoS_2 and $MoSe_2$ Thin Films. *ACS Appl. Mater. Interfaces* **2016**, *8*, 31442−31448.
(52) Mattila, S.; Leiro, J. A.; Heinonen, M.; Laiho, T. Core Level Spectroscopy of MoS_2. *Surf. Sci.* **2006**, *600*, 5168−5175.
(53) Cao, D.; Shen, T.; Liang, P.; Chen, X.; Shu, H. Role of Chemical Potential in Flake Shape and Edge Properties of Monolayer MoS_2. *J. Phys. Chem. C* **2015**, *119*, 4294−4301.
(54) Bruix, A.; Füchtbauer, H. G.; Tuxen, A. K.; Walton, A. S.; Andersen, M.; Porsgaard, S.; Besenbacher, F.; Hammer, B.; Lauritsen, J. V. In Situ Detection of Active Edge Sites in Single-Layer MoS_2 Catalysts. *ACS Nano* **2015**, *9*, 9322−9330.
(55) Lassalle-Kaiser, B.; Merki, D.; Vrubel, H.; Gul, S.; Yachandra, V. K.; Hu, X.; Yano, J. Evidence from in Situ X-Ray Absorption Spectroscopy for the Involvement of Terminal Disulfide in the

DOI: 10.1021/acsami.8b07489
ACS Appl. Mater. Interfaces 2018, 10, 27771−27779

Reduction of Protons by an Amorphous Molybdenum Sulfide Electrocatalyst. *J. Am. Chem. Soc.* **2015**, *137*, 314−321.
(56) Deng, Y.; Yeo, B. S. Characterization of Electrocatalytic Water Splitting and CO_2 Reduction Reactions Using in Situ/Operando Raman Spectroscopy. *ACS Catal.* **2017**, *7*, 7873−7889.
(57) Deng, Y.; Ting, L. R. L.; Neo, P. H. L.; Zhang, Y.-J.; Peterson, A. A.; Yeo, B. S. Operando Raman Spectroscopy of Amorphous Molybdenum Sulfide (MoS_x) During the Electrochemical Hydrogen Evolution Reaction: Identification of Sulfur Atoms as Catalytically Active Sites for H^+ Reduction. *ACS Catal.* **2016**, *6*, 7790−7798.

DOI: 10.1021/acsami.8b07489
ACS Appl. Mater. Interfaces 2018, 10, 27771−27779